Aegean Sea as driver of hydrographic and ecological changes in the eastern Mediterranean

Gianluca Marino* Institute for Coastal Marine Environment, National Research Council, Porto di Napoli, Calata Porta di Massa, 80133 Naples, Italy
Eelco J. Rohling National Oceanography Centre, Southampton, Hampshire SO14 3ZH, UK
W. Irene C. Rijpstra Department of Marine Biogeochemistry and Toxicology, Royal Netherlands Institute for Sea Research, PO Box 59, Den Burg, Texel, Netherlands
Francesca Sangiorgi Palaeoecology, Institute of Environmental Biology, Laboratory of Palaeobotany and Palynology, Utrecht University, Budapestlaan 4, 3584 CD Utrecht, Netherlands, and Department of Marine Biogeochemistry and Toxicology, Royal Netherlands Institute for Sea Research, PO Box 59, Den Burg, Texel, Netherlands
Stefan Schouten, Jaap S. Sinninghe Damsté — Department of Marine Biogeochemistry and Toxicology, Royal Netherlands Institute for Sea Research, PO Box 59, Den Burg, Texel, Netherlands

ABSTRACT

The eastern Mediterranean is undergoing a long-term increase in net evaporation, which may have preconditioned the profound changes that occurred in its deep-sea ventilation over the past two decades. We test the sensitivity of Aegean convective deep-water formation to forcing in the opposite sense, based on a last interglacial episode of enhanced freshwater injection into the eastern Mediterranean. We find that Aegean subsurface ventilation collapsed completely within 40 ± 20 yr, promoting euxinic conditions hostile to aerobic life that expanded toward the photic layer within 650 ± 250 yr. Similar conditions extended throughout the eastern Mediterranean 300 ± 120 yr later. These findings emphasize the exceptional sensitivity of Aegean deep-water formation to climate forcing, driving large-scale hydrographic adjustments throughout the eastern Mediterranean and beyond.

Keywords: Mediterranean Sea, thermohaline circulation, sapropels, stable isotopes, biomarkers.

INTRODUCTION

On a global scale, new deep-water formation delivers oxygen to the deep sea. In the eastern Mediterranean, this process has long been dominated by the sinking and spreading of Adriatic dense waters (Malanotte-Rizzoli and Hecht, 1988). In the late 1980s–early 1990s, there was an abrupt shift to dominance of Aegean deep waters in the eastern Mediterranean deep-sea ventilation (Eastern Mediterranean Transient) (Roether et al., 1996; Klein et al., 1999; Malanotte-Rizzoli et al., 1999) that eventually influenced even the density of Mediterranean outflow into the Atlantic (Millot et al., 2006). Several studies conclude that this profound hydrographic reorganization was preconditioned by a long-term increase in eastern Mediterranean net evaporation (Béthoux et al., 1998; Boscolo and Bryden, 2001; Skliris and Lascaratos, 2004; Skliris et al., 2007). Other studies emphasize the role of synoptic changes in the wind field affecting upper thermocline circulation and, in turn, the salt supply to the Aegean Sea (Malanotte-Rizzoli et al., 1999; Samuel et al., 1999; Stratford and Haines, 2002).

We investigate the sensitivity of the Aegean thermohaline circulation to a reduction of eastern Mediterranean net evaporation due to freshwater flooding, using a key example of the organic-rich layers (sapropels) that periodically occur in the eastern Mediterranean sedimentary archive. Sapropels reflect periods of sluggish bottom-water ventilation in response to enhanced monsoon-fueled river discharge along the North African margin (e.g., Rohling et al., 2002; Emeis et al., 2003). Last interglacial sapropel S5 is intensely developed and holds excellent potential for high-resolution studies (Cane et al., 2002; Rohling et al., 2002, 2004, 2006). However, a lack of Aegean S5 records has, to date, limited our understanding of the hydrographic responses in this critical region to a sharp reduction in eastern Mediterranean net evaporation.

Here we present the first systematic high-resolution multiproxy study of an Aegean S5, as retrieved from southeastern Aegean core LC21 (Fig. 1). Results are discussed within the context of previously described contemporaneous records from the open eastern Mediterranean Ocean Drilling Program (ODP) Site 971A (Cane et al., 2002; Rohling et al., 2002, 2004, 2006).

MATERIAL AND METHODS

Core LC21 was recovered in 1995 by RV *Marion Dufresne* for the EC-MAST2 (Marine, Science, and Technology Programme) PALAEOFLUX (Biogeochemical Fluxes in the Mediterranean Water-Sediment System) program. We analyzed S5, in sections 5 and 6, at 1 cm (decadal) resolution for $\delta^{18}O$ and $\delta^{13}C$ in *Globigerinoides ruber* (white) and *Neogloboquadrina pachyderma* (dextral), and at 5 cm (centennial) resolution for alkenone-based sea surface temperatures (SSTs), total organic carbon (C_{org}), and isorenieratene concentrations (GSA Data Repository Fig. DR1[1]).

Stable isotope analyses were performed in Southampton with a Europa Geo2020 dual inlet mass spectrometer following individual acid-bath reaction of 15–20 handpicked and cleaned specimens in the size ranges 300–350 m (*G. ruber*) and 250–300 m (*N. pachyderma*). Isotope ratios are expressed as $\delta^{13}C$ and $\delta^{18}O$, in permil values relative to Vienna Peedee belemnite (VPDB). External precision was better than 0.06‰ for both $\delta^{13}C$ and $\delta^{18}O$.

The C_{org} contents, alkenone analyses, and isorenieratene concentrations were performed at the Royal Netherlands Institute for Sea Research. The C_{org} contents were determined on decalcified sediments, using a Carlo Erba Flash elemental analyzer coupled to a Thermofinnigan DeltaPLUS isothermal remanent magnetization mass spectrometer (MS) system. For alkenone analysis, freeze-dried and homogenized sediments were extracted using the Dionex accelerated solvent extraction (ASE) technique using dichloromethane (DCM)/methanol (2:1, v/v) at 100 °C and 7.6×10^6 Pa. The extracts were separated by Al_2O_3 column chromatog-

*E-mail: G.Marino@uu.nl; Currently also at Palaeoecology, Institute of Environmental Biology, Laboratory of Palaeobotany and Palynology, Utrecht University, Budapestlaan 4, 3584 CD Utrecht, Netherlands.

[1]GSA Data Repository item 2007175, Appendix DR1 and Figures DR1 and DR2, (supplementary information on stratigraphic framework and chronology) is available online at www.geosociety.org/pubs/ft2007.htm, or on request from editing@geosociety.org or Documents Secretary, GSA, P.O. Box 9140, Boulder, CO 80301, USA.

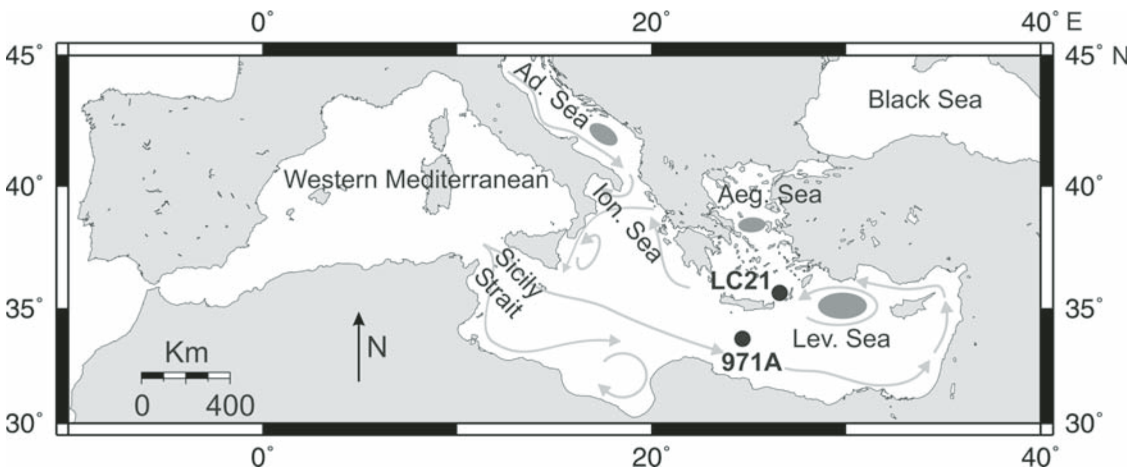

Figure 1. Map of Mediterranean showing main patterns of surface circulation (gray arrows), sites of eastern Mediterranean dense water formation (shaded areas) (Pinardi and Masetti, 2000), and locations (black dots) of core LC21 (35°40′N, 26°35′E; 1522 m water depth) and Ocean Drilling Program Site 971A (33°43′N; 24°41′E; 2026 m water depth). Aeg.—Aegean; Lev.—Levantine; Ad.—Adriatic; Ion.—Ionian.

raphy using first hexane/DCM (9:1, v/v) and then hexane/DCM (1:1, v/v) to elute the alkenone fraction, which was analyzed by gas chromatography (GC) and GC/MS. Alkenone-based SSTs were calculated following Müller et al. (1998). Isorenieratene concentrations were determined following Hopmans et al. (2005).

RESULTS AND DISCUSSION

Sapropel S5 in LC21 is the most intensely developed sapropel known from the Pleistocene, with C_{org} concentrations as high as 14% and a thickness of ~120 cm (Fig. DR1), deposited over a period of ~5 k.y. (e.g., Rohling et al., 2002). The absence of benthic fossils, the preserved sedimentary lamination in several intervals, and the occurrence of specific biomarkers (see following) together indicate euxinic conditions in the Aegean water column during S5 deposition. In the absence of bioturbation, the great thickness of S5 in LC21 allows very high sampling resolution.

We compare our results for S5 from Aegean core LC21 with those from open eastern Mediterranean ODP Site 971A (Fig. 1). Using the statistical multiproxy correlation approach for records through S5 (Cane et al., 2002; Rohling et al., 2002), the LC21 record has been transferred onto the 971A-equivalent depth scale that serves as a master depth scale for S5 in the open eastern Mediterranean (Appendix DR1 and Fig. DR1). This method allows a direct comparison between signals recorded in Aegean core LC21 and those in open eastern Mediterranean ODP Site 971A, with a vertical uncertainty of less than ±1 cm ($1\sigma = \pm 0.83$ cm) within S5 on the 971A-equivalent depth scale. This correlation indicates an exact coincidence of the large shift to light $\delta^{18}O_{ruber}$ near the onset of S5 in the two cores (Fig. 2B). Given the basin's prevalent wind-driven surface circulation and the proximity of the two sites (<300 km), such a large and abrupt signal is expected to be synchronous within the 40 ± 20 yr temporal resolution of our record. We are therefore confident that our statistical method delimits the correlations well within the 1σ bounds for this crucial segment of the records.

Our chronology for S5 relies on a simple linear interpolation between the estimated ages of the onset and termination of the associated light $\delta^{18}O_{ruber}$ anomaly (Rohling et al., 2002), suggesting that, within S5, 1 cm corresponds to ~40 ± 20 yr in LC21 and ~200 ± 80 yr in 971A (Appendix DR1). The sediment mass accumulation rate (SMAR) in LC21 exceeds that in 971A by 5 times. Given this SMAR difference and that C_{org} concentrations reach 14% in LC21 compared to 7% in 971A, it appears that the C_{org} burial flux during S5 deposition was a full order of magnitude higher in the Aegean Sea than in the open eastern Mediterranean.

Figure 2 shows the signals through S5 in LC21 along with their counterparts in ODP Site 971A (all data on the common 971A depth scale). At both sites, the absolute $\delta^{18}O_{pachyderma}$ values are virtually identical (Fig. 2C). This supports the previous notion that the isotopic composition of *N. pachyderma* reflects basin-integrated property changes, suggesting a habitat in (top) intermediate waters deriving from a single source region (Rohling et al., 2004). In Aegean core LC21, changes in $\delta^{18}O_{ruber}$ appear to closely track $\delta^{18}O_{pachyderma}$ within S5, which contrasts with strong variable offsets between $\delta^{18}O_{ruber}$ and $\delta^{18}O_{pachyderma}$ in 971A (Fig. DR2). The $\delta^{18}O_{ruber}$ represents near-surface conditions in the summer mixed layer (Rohling et al., 2004), and the similarity between $\delta^{18}O_{ruber}$ and $\delta^{18}O_{pachyderma}$ in LC21 suggests that both species inhabited water masses with similar properties. This would agree with modern observations that the southeastern Aegean site of LC21 is directly in the northward flow path of Levantine surface water (Theocharis et al., 2002), which derives from the area where Levantine intermediate water is formed, and that the intermediate water reaches depths as shallow as 70 m in the Aegean due to prevailing northerly winds and the basin's general cyclonic circulation (Poulos et al., 1997; Pinardi and Masetti, 2000; Zervakis et al., 2004). Work on the Holocene period of S1 deposition indicates similar conditions during times of decreased eastern Mediterranean net evaporation (Myers et al., 1998; Casford et al., 2002).

Given that the $\delta^{18}O_{pachyderma}$ records through S5 are similar for both sites, the contrast between $\delta^{18}O_{ruber}$ and $\delta^{18}O_{pachyderma}$ in 971A can be entirely attributed to variability in $\delta^{18}O_{ruber}$. The $\delta^{18}O_{ruber}$ signal in 971A displays lighter values (the offset from $\delta^{18}O_{pachyderma}$ reaches more than 1.5‰; Fig. DR2) and also is more variable than in LC21 (Fig. 2B). Because both sites have similar SSTs (Fig. 2A), this difference in $\delta^{18}O_{ruber}$ is unlikely to be attributable to SST contrasts. The $\delta^{18}O_{ruber}$ differences within S5 contrast with the similarity of $\delta^{18}O_{ruber}$ at the two sites before and after S5. The observed differences between the $\delta^{18}O_{ruber}$ signals within S5, along with similarity of $\delta^{18}O_{pachyderma}$ and SST signals in LC21 and 971A as well as other sites throughout the eastern Mediterranean (Rohling et al., 2002), may only be explained by limited interaction between surface and intermediate waters at the location of Site 971A, which is remote from the intermediate-water source region.

Spatially, $\delta^{18}O_{ruber}$ is lighter around the location of 971A than elsewhere in the open eastern Mediterranean (Rohling et al., 2002), as observed for other sapropels (Rohling and De Rijk, 1999; Emeis et al., 2003). This pattern has been ascribed to extensive (monsoon fueled) freshwater drainage along the wider North African margin, through currently dry river (wadi) systems, supplementing—but more variable than—Nile River discharge (Rohling et al., 2002, 2004; Scrivner et al., 2004). The $\delta^{18}O_{ruber}$ values in the brief interval of reduced discharge (Rohling et al., 2002) from the wider North African margin (56–52 cm in 971A) decrease back to the typical $\delta^{18}O_{ruber}$ values found throughout S5 in LC21 (Fig. 2B). This suggests that the Aegean record reflects an underlying $\delta^{18}O_{ruber}$ controlled by less intense freshwater dilution that may reflect propagation through the basin of the surface freshening caused by North African river input into the open eastern Mediterranean (Rohling et al., 2002; Scrivner

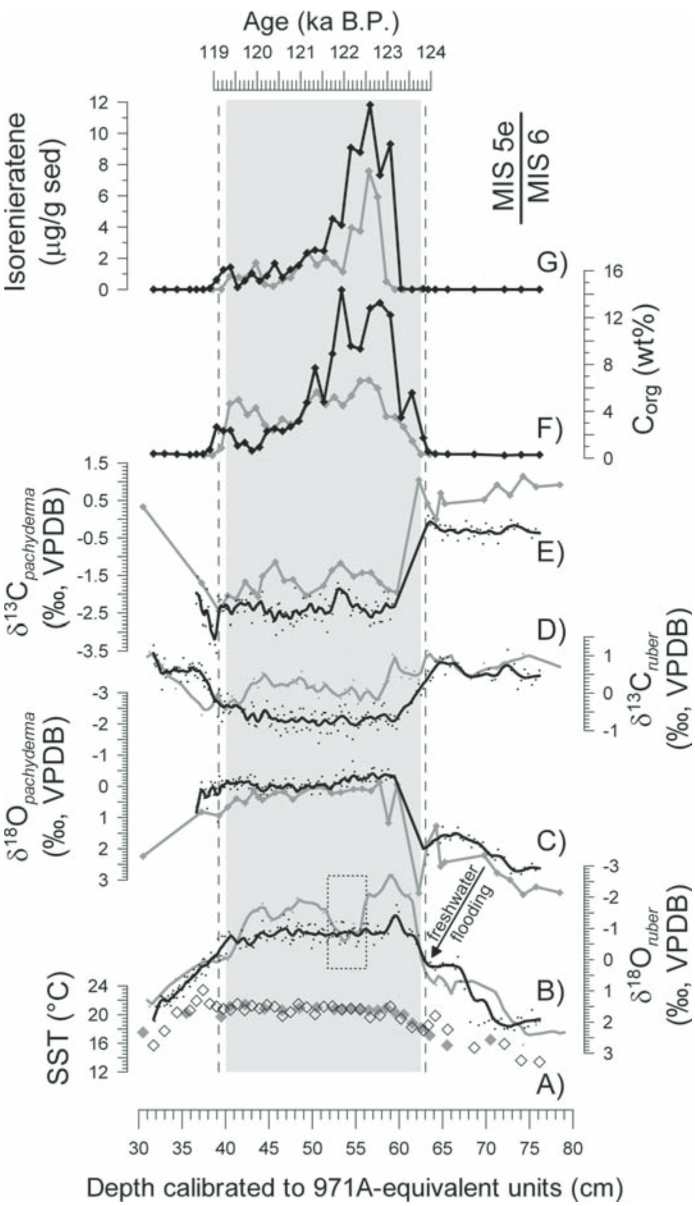

Figure 2. Geochemical proxies through S5 in core LC21 (black lines and symbols) and core 971A (gray lines and symbols). A: Alkenone-based sea suface temperature (SST) reconstructions. Alkenones today are produced by coccolithophores that bloom in winter and/or spring in the eastern Mediterranean (Ziveri et al., 2000). SST axis is calibrated relative to $\delta^{18}O$ axis so that every 1 °C change in temperature corresponds to 0.23‰ in $\delta^{18}O$ (Kim and O'Neil, 1997). B, C: $\delta^{18}O$ records for *Globigerinoides ruber* and *Neogloboquadrina pachyderma*, respectively. D, E: $\delta^{13}C$ records for *G. ruber* and *N. pachyderma*, respectively. Isotopic records (B, C, D, and E) were loess smoothed (solid lines) (tension 0.04 and 0.05, respectively). F: Organic carbon (C_{org}) contents. G: Isorenieratene abundances. All profiles are plotted vs. 971A-equivalent depth scale. Gray shaded area and dashed lines represent visual extent of dark-colored sapropel S5 sediments in 971A and in LC21, respectively. Dotted inset identifies $\delta^{18}O_{ruber}$ (heavy) anomaly in core 971A (Rohling et al., 2002). Age scale (right) is based on linear interpolation between estimated ages of 124 and 119 ka B.P. for depletion and enrichment trends in $\delta^{18}O_{ruber}$ preceding and following S5 onset and end, respectively. MIS—marine oxygen isotope stage; VPDB—Vienna Peedee belemnite.

et al., 2004). Superimposed on this widespread average mixed signal, the large regional $\delta^{18}O_{ruber}$ anomalies found in the open eastern Mediterranean (notably near 971A) would reflect more direct impacts of the river-borne monsoon floods.

LC21 and 971A simultaneously reach the lightest $\delta^{18}O_{ruber}$ values ~650 ± 250 yr after the sharp $\delta^{18}O_{ruber}$ shift that marks the onset of freshwater flooding into the basin (Fig. 2B). This peak in eastern Mediterranean sea-surface freshening coincides with the appearance of very light $\delta^{13}C_{pachyderma}$ values (lighter by ~2‰ than $\delta^{13}C_{ruber}$; Fig. DR2) at both sites, following ~400 yr of near absence of this species throughout the eastern Mediterranean (Rohling et al., 2006). The shift to light $\delta^{13}C_{pachyderma}$ values, observed in both records, has been suggested to reflect the proximity of a subsurface reservoir of isotopically light metabolized carbon to the subsurface habitat of *N. pachyderma* (Rohling et al., 2006). At the same level in LC21, high concentrations appear of isorenieratene (>9 g/g sediment), a specific aromatic carotenoid of anaerobic, photolithotrophic green sulfur bacteria (Chlorobiaceae) (Fig. 2G). These bacteria require both sulfide and light (Repeta et al., 1989; Koopmans et al., 1996; Passier et al., 1999). Similar to the reconstruction for the open eastern Mediterranean (Rohling et al., 2006), the abrupt appearance of high isorenieratene concentrations in the Aegean Sea, combined with the occurrence of subthermocline foraminiferal species (e.g., *N. pachyderma*), reflects the development of euxinic conditions throughout the Aegean water column up to ~200 m. Comparison of LC21 with 971A (Fig. 2G) illustrates that such conditions had developed in the Aegean Sea 100 ± 40 to 300 ± 120 yr before they became established in the open eastern Mediterranean.

A clear sequence of causes and effects can now be summarized for the last interglacial episode of freshwater flooding into the eastern Mediterranean. Given that benthic azoic conditions and a sharp C_{org} increase developed immediately following the onset of surface freshening (from one sample to the next in LC21), we infer that Aegean ventilation collapsed completely within 40 ± 20 yr in response to the change in hydrological forcing, even though most of the hydrological change was driven by monsoon flooding into the open eastern Mediterranean rather than centered on the Aegean Sea. Increased preservation of C_{org} due to oxygen starvation (Moodley et al., 2005), first at the seafloor and then rapidly throughout the water column (Bianchi et al., 2006), would (partly) explain the large jump in the C_{org} record (Fig. 2F). Within ~650 yr, euxinic conditions expanded through the Aegean water column to depths of 200 m or less, fueling populations of Chlorobiaceae, with concomitant shoaling of the reservoir of isotopically light metabolized carbon into the habitat of *N. pachyderma*. Euxinic conditions reached similar depths in the open eastern Mediterranean~100–300 yr later (Fig. 2G).

CONCLUSIONS

Our results highlight an intriguing similarity in the time scale of Aegean response to climate forcing between the recent and the last interglacial events. In the mid-1960s, construction of major dams (e.g., Aswan High Dam) initiated a relatively long term (estimated 80 yr) adjustment in the basin to the effects of enhanced net evaporation (Rohling and Bryden, 1992). This has been proposed as an important multidecadal preconditioning for the modern eastern Mediterranean hydrographic changes (Boscolo and Bryden, 2001; Skliris and Lascaratos, 2004; Skliris et al., 2007). Here we find that another dramatic Aegean-focused response occurred during the last interglacial within a similar period of time (<40 ± 20 yr), although this concerns a perturbation in the eastern Mediterranean freshwater budget of the opposite sign.

Combined with the instrumental record of the Eastern Mediterranean Transient, our findings for the S5 period highlight an exceptional sensitivity of the Aegean to changes in wider eastern Mediterranean climate forcing of any sign, with responses that lead to profound hydrographic adjustments that subsequently propagate throughout the open eastern Mediterranean, and that potentially affect even the North Atlantic (Millot et al., 2006). Both increases (preconditioning modern changes) and decreases (this study) in eastern Mediterranean net evaporation are found to drive basin-scale reorganizations in subsurface water-mass dynamics, with extensive ecological impacts.

ACKNOWLEDGMENTS

This study has been supported by the UK Natural Environmental Research Council, Netherlands Organization for Scientific Research, and Institute for Coastal Marine Environment, National Research Council. H. Brinkhuis, B. D'Argenio, M. Ribera d'Alcalà, A. Lotter, and three anonymous reviewers helped to improve the manuscript. We thank M. Bolshaw, E. Hopmans, and J. Ossebaar for their assistance. This study contributes to the Marine Science and Engineering Doctorate, Federico II University, Naples, Italy, and to MEDCLIVAR (Mediterranean Climate Variability and Predictability).

REFERENCES CITED

Béthoux, J.-P., Gentili, B., and Tailliez, D., 1998, Warming and freshwater budget changes in the Mediterranean since the 1940s: Their possible relation to the greenhouse effect: Geophysical Research Letters, v. 25, p. 1023–1026, doi: 10.1029/98GL00724.

Bianchi, D., Zavatarelli, M., Pinardi, N., Capozzi, R., Capotondi, L., Corselli, C., and Masina, S., 2006, Simulations of ecosystem response during the sapropel S1 deposition event: Palaeogeography, Palaeoclimatology, Palaeoecology, v. 235, p. 265–287, doi: 10.1016/j.palaeo.2005.09.032.

Boscolo, R., and Bryden, H., 2001, Causes of long-term changes in the Aegean Sea deep water: Oceanologica Acta, v. 24, p. 519–527, doi: 10.1016/S0399–1784(01)01172–0.

Cane, T., Rohling, E.J., Kemp, A.E.S., Cooke, S., and Pearce, R.B., 2002, High-resolution stratigraphic framework for Mediterranean sapropel S5: Defining temporal relationships between records of Eemian climate variability: Palaeogeography, Palaeoclimatology, Palaeoecology, v. 183, p. 87–101, doi: 10.1016/S0031–0182(01)00461–8.

Casford, J.S.L., Rohling, E.J., Abu-Zied, R., Cooke, S., Fontanier, C., Leng, M., and Lykousis, V., 2002, Circulation changes and nutrient concentrations in the late Quaternary Aegean Sea: A nonsteady state concept for sapropel formation: Paleoceanography, v. 17, p. 1024, doi: 10.1029/2000PA000601.

Emeis, K.-C., Schulz, H., Struck, U., Rossignol-Strick, M., Erlenkeuser, H., Howell, M.W., Kroon, D., Mackensen, H., Ishizuka, S., Oba, T., Sakamoto, T., and Koizumi, I., 2003, Eastern Mediterranean surface water temperatures and $\delta^{18}O$ composition during deposition of sapropels in the late Quaternary: Paleoceanography, v. 18, p. 1005, doi: 10.1029/2000PA000617.

Hopmans, E.C., Schouten, S., Rijpstra, W.I.C., and Sinninghe Damsté, J.S., 2005, Identification of carotenals in sediments: Organic Geochemistry, v. 36, p. 485–495, doi: 10.1016/j.orggeochem.2004.10.001.

Kim, S.T., and O'Neil, J.R., 1997, Equilibrium and nonequilibrium oxygen isotope effects in synthetic calcites: Geochimica et Cosmochimica Acta, v. 61, p. 3461–3475, doi: 10.1016/S0016–7037(97)00169–5.

Klein, B., Roether, W., Manca, B.B., Bregant, D., Beitzel, V., Kovacevic, V., and Luchetta, A., 1999, The large deep water transient in the eastern Mediterranean: Deep-Sea Research, v. 46, p. 371–414, doi: 10.1016/S0967–0637(98)00075–2.

Koopmans, M.P., Köster, J., Van Kaam-Peters, H.M.E., Kenig, F., Schouten, S., Hartgers, W.A., De Leeuw, J.W., and Sinninghe Damsté, J.S., 1996, Diagenetic and catagenetic products of isorenieratene: Molecular indicators for photic zone anoxia: Geochimica et Cosmochimica Acta, v. 60, p. 4467–4496, doi: 10.1016/S0016–7037(96)00238–4.

Malanotte-Rizzoli, P., and Hecht, A., 1988, Large-scale properties of the eastern Mediterranean: A review: Oceanologica Acta, v. 11, p. 323–335.

Malanotte-Rizzoli, P., Manca, B.B., Ribera d'Alcala, M., Theocharis, A., Brenner, S., Budillon, G., and Ozsoy, E., 1999, The Eastern Mediterranean in the 80s and in the 90s: The big transition in the intermediate and deep circulations: Dynamics of Atmospheres and Oceans, v. 29, p. 365–395, doi: 10.1016/S0377–0265(99)00011–1.

Millot, C., Candela, J., Fuda, J.L., and Tber, Y., 2006, Large warming and salinification of the Mediterranean outflow due to changes in its composition: Deep-Sea Research, v. 53, p. 656–666, doi: 10.1016/j.dsr.2005.12.017.

Moodley, L., Middelburg, J.J., Herman, P.M.J., Soetaert, K., and de Lange, G.J., 2005, Oxygenation and organic-matter preservation in marine sediments: Direct experimental evidence from ancient organic carbon–rich deposits: Geology, v. 33, p. 889–892, doi: 10.1130/G21731.1.

Müller, P.J., Kirst, G., Ruhland, G., von Storch, I., and Rosell-Mélé, A., 1998, Calibration of the alkenone paleotemperature index $U^{k'}_{37}$ based on core tops from the eastern South Atlantic and the global ocean (60°N–60°S): Geochimica et Cosmochimica Acta, v. 62, p. 1757–1772, doi: 10.1016/S0016–7037(98)00097–0.

Myers, P.G., Haines, K., and Rohling, E.J., 1998, Modelling the paleo-circulation of the Mediterranean: The last glacial maximum and the Holocene with emphasis on the formation of sapropel S1: Paleoceanography, v. 13, p. 586–606, doi: 10.1029/98PA02736.

Passier, H.F., Bosch, H.-J., Nijenhuis, I.A., Lourens, L.J., Bottcher, M.E., Leenders, A., Sinninghe Damsté, J.S., De Lange, G.J., and De Leeuw, J.W., 1999, Sulphidic Mediterranean surface waters during Pliocene sapropel formation: Nature, v. 397, p. 146–149, doi: 10.1038/16441.

Pinardi, N., and Masetti, E., 2000, Variability of the large scale general circulation of the Mediterranean Sea from observations and modelling: A review: Palaeogeography, Palaeoclimatology, Palaeoecology, v. 158, p. 153–173, doi: 10.1016/S0031–0182(00)00048–1.

Poulos, S.E., Drakopoulos, P.G., and Collins, M.B., 1997, Seasonal variability in sea surface oceanographic conditions in the Aegean Sea (eastern Mediterranean): An overview: Journal of Marine Systems, v. 13, p. 225–244, doi: 10.1016/S0924–7963(96)00113–3.

Repeta, D.J., Simpson, D.J., Jørgensen, B.B., and Jannasch, H.W., 1989, Evidence for anoxygenic photosynthesis from the distribution of bacteriochlorophylls in the Black Sea: Nature, v. 342, p. 69–72, doi: 10.1038/342069a0.

Roether, W., Manca, B.B., Klien, B., Bregant, D., Georgopoulos, D., Beitzel, V., Kovacevic, V., and Luchetta, A., 1996, Recent changes in Eastern Mediterranean Deep Waters: Science, v. 271, p. 333–335, doi: 10.1126/science.271.5247.333.

Rohling, E.J., and Bryden, H.L., 1992, Man-induced salinity and temperature increases in western Mediterranean Deep Water: Journal of Geophysical Research, v. 97, p. 11,191–11,198.

Rohling, E.J., and De Rijk, S., 1999, The Holocene Climate Optimum and Last Glacial Maximum in the Mediterranean: The marine oxygen isotope record: Marine Geology, v. 153, p. 57–75, doi: 10.1016/S0025–3227(98)00020–6.

Rohling, E.J., Cane, T.R., Cooke, S., Sprovieri, M., Bouloubassi, I., Emeis, K.-C., Schiebel, R., Kroon, D., Jorissen, F.J., Lorre, A., and Kemp, A.E.S., 2002, African monsoon variability during the previous interglacial maximum: Earth and Planetary Science Letters, v. 202, p. 61–75, doi: 10.1016/S0012–821X(02)00775–6.

Rohling, E.J., Sprovieri, M., Cane, T.R., Casford, J.S.L., Cooke, S., Bouloubassi, I., Emeis, K.C., Schiebel, R., Rogerson, M., Hayes, A., Jorissen, F.J., and Kroon, D., 2004, Reconstructing past planktic foraminiferal habitats using stable isotope data: A case history for Mediterranean sapropel S5: Marine Micropaleontology, v. 50, p. 89–123, doi: 10.1016/S0377–8398(03)00068–9.

Rohling, E.J., Hopmans, E.C., and Sinninghe Damsté, J.S., 2006, Water column dynamics during the last interglacial anoxic event in the Mediterranean (sapropel S5): Paleoceanography, v. 21, p. PA2018, doi: 10.1029/2005PA001237.

Samuel, S., Haines, K., Josey, S., and Myers, P.G., 1999, Response of the Mediterranean Sea thermohaline circulation to observed changes in the winter wind stress field in the period 1980–1993: Journal of Geophysical Research, v. 104, p. 7771–7784, doi: 10.1029/1998JC900130.

Scrivner, A., Vance, D., and Rohling, E.J., 2004, New neodymium isotope data quantify Nile involvement in Mediterranean anoxic episodes: Geology, v. 32, p. 565–568, doi: 10.1130/G20419.1.

Skliris, N., and Lascaratos, A., 2004, Impacts of the Nile River damming on the thermohaline circulation and water mass characteristics of the Mediterranean Sea: Journal of Marine Systems, v. 52, p. 121–143, doi: 10.1016/j.jmarsys.2004.02.005.

Skliris, N., Sofianos, S., and Lascaratos, A., 2007, Hydrological changes in the Mediterranean Sea in relation to changes in the freshwater budget: A numerical modelling study: Journal of Marine Systems, v. 65, p. 400–416, doi: 10.1016/j.jmarsys.2006.01.015.

Stratford, K., and Haines, K., 2002, Modelling changes in Mediterranean thermohaline circulation 1987–1995: Journal of Marine Systems, v. 33–34, p. 51–62, doi: 10.1016/S0924–7963(02)00052–0.

Theocharis, A., Klein, B., Nittis, K., and Roether, W., 2002, Evolution and status of the Eastern Mediterranean Transient (1997–1999): Journal of Marine Systems, v. 33–34, p. 91–116, doi: 10.1016/S0924–7963(02)00054–4.

Zervakis, V., Georgopoulos, D., Karageorgis, A.P., and Theocharis, A., 2004, On the response of the Aegean sea to climatic variability: A review: International Journal of Climatology, v. 24, p. 1845–1858, doi: 10.1002/joc.1108.

Ziveri, P., Ruten, A., de Lange, G.J., Thomson, J., and Corselli, C., 2000, Present-day coccolith fluxes recorded in central eastern Mediterranean sediment traps and surface sediments: Palaeogeography, Palaeoclimatology, Palaeoecology, v. 158, p. 175–195, doi: 10.1016/S0031–0182(00)00049–3.

Manuscript received 24 February 2007
Revised manuscript received 16 March 2007
Manuscript accepted 17 March 2007

Printed in USA

Data Repository Material: The Aegean Sea as driver of hydrographic and ecological changes in the eastern Mediterranean

by **Marino et al.**

Appendix DR1: Supplementary Information on stratigraphic framework and chronology

Stratigraphic framework

The approach we use to build a stratigraphic framework for core LC21 statistically seeks the best correlation with ODP core 971A, which was previously proposed as “master record” for S5 in the eastern Mediterranean (eMed) (Cane et al., 2002). In this correlation none of the correlation markers were a priori assumed to be syn-/diachronous. Distinct and unambiguously defined stratigraphic markers based on five independent proxy records have been recognized on a basin scale during the S5 deposition (Figure DR1, panel II). Remarkable O and C isotope shifts, clear faunal presence/absence and sharp peaks in the C_{org} and isorenieratene abundance have been recognized in Aegean LC21 and western Levantine 971A (Figure DR1, Table DR1). Markers, such as faunal zero abundance levels of the most abundant foraminiferal species, and sharp peaks in the isotopic profiles have been assigned a primary role, and these were used to establish the correlation between the two sites. Markers deriving from less well-defined events, and shifts in organic carbon content and isorenieratene abundance have been assigned a secondary role and were used for validation of the regression only. In order to avoid possible bias caused by post-depositional oxidation, the visual extent of the dark-coloured sapropel sediments was not used to identify the calibration (Cane et al., 2002).

In Figure DR1 (panel II), 11 primary (grey open diamonds) and the 12 secondary (black solid circles) correlation marker pairs for LC21 and 971A are plotted against one-another. Linear regression between primary correlation markers is highly significant (R^2=0.97). Moreover, the regression is corroborated by the proximity of the secondary markers to the linear fit. Nevertheless, a second-order polynomial regression between primary correlation markers (R^2=0.996), albeit statistically indistinct from the linear regression, yields a visual "point to point" improvement. Therefore, the latter regression has been employed to calibrate the LC21 depth scale to 971A-equivalent depths. The 1σ uncertainty that applies to the correlation based on the second-order polynomial fit through the primary correlation markers equals ±0.83 cm.

Chronology

The results presented here support the concept of a non-synchronous inception of anoxic conditions throughout the basin during the last interglacial period (Cane et al., 2002). In contrast, the onset of the monsoon-fuelled freshwater dilution of the eMed surface waters has been virtually synchronous throughout the basin, preceding the organic-rich sedimentation (Rohling et al., 2002a). Since the eMed sea surface is the principal source of moisture for precipitation over Soreq Cave (N. Israel) (Matthews et al., 2000), any appreciable change in the oxygen isotopic composition of eMed sea surface waters (as reflected in $\delta^{18}O_{ruber}$) will be recorded directly by a comparable shift in the $\delta^{18}O_{\mathrm{calcite}}$ of Soreq Cave speleothems (Bar-Matthews et al., 2000). Therefore, in agreement with Rohling et al. (2002a), we contend that the onset of the humid phase in the eMed region during the Marine Isotopic Stage 5e (MIS 5e) is synchronous at a basin-scale and can be assigned an approximate age of 124 ka B.P (Bar-Matthews et al., 2000). Similarly, the major return of $\delta^{18}O_{ruber}$ to pre-sapropel values near the end of S5 deposition is synchronous between LC21 and 971A and throughout the eMed (Rohling et al., 2002a), and matches the termination of the humid phase in Soreq Cave dated at around 119 ka B.P. (Bar-Matthews et al., 2000).

The chronology for S5 provided in the present study relies on a simple linear interpolation (i.e. assuming a constant sedimentation rate throughout the S5) between the estimated ages of the onset (124 ka B.P.) and the termination (119 ka B.P.) of the depletion and enrichment trends in $\delta^{18}O_{ruber}$. On the basis of this very simple calculation, and taking into account a 2 k.y. uncertainty in the duration of the humid period in Soreq Cave (Bar-Matthews et al., 2000), 1 cm corresponds to 39.7±20 years in core LC21, and 199.4±80 years in core 971A. An analogous coincidence between major shifts in

$\delta^{18}O_{calcite}$ of the Soreq Cave speleothems and in $\delta^{18}O_{ruber}$ in LC21 (Rohling et al., 2002b) is associated with a widespread humid event at the time of deposition of early- to mid-Holocene sapropel S1 (see also Arz et al., 2003). The timing relationship between LC21 and Soreq Cave during the early- to mid-Holocene is supported by independent datings performed on both archives (Bar-Matthews et al., 2000; Mercone et al., 2000), and the close agreement between those results corroborates our approach of using the datings from Soreq Cave to provide a chronology for sapropel S5.

Additional references

Arz, H. W., Lamy, F., Pätzold, J., Müller, P. J., and Prins, M, 2003, Mediterranean moisture source for an early-Holocene humid period in the Northern Red Sea: Science, v. 300, p. 118–121, doi: 10.1126/science.1080325.

Bar-Matthews, M., Ayalon, A., and Kaufman, A, 2000, Timing and hydrological conditions of Sapropel events in the Eastern Mediterranean, as evident from speleothems, Soreq cave, Israel: Chemical Geology, v. 169, p. 145–156, doi:10.1016/S0009-2541(99)00232-6.

Cane, T., Rohling, E.J., Kemp, A.E.S., Cooke, S., and Pearce, R.B., 2002, High-resolution stratigraphic framework for Mediterranean sapropel S5: defining temporal relationships between records of Eemian climate variability: Palaeogeography, Palaeoclimatology, Palaeoecology, v. 183, p. 87–101, doi: 10.1016/S0031–0182(01)00461–8.

Matthews, A., Ayalon, A., and Bar-Matthews, M., 2000, D/H ratios of fluid inclusions of Soreq Cave (Israel) speleothems as a guide to the Eastern Mediterranean Meteoric Line relationships in the last 120 ky: Chemical Geology, v. 166, 183–191, doi:10.1016/S0009-2541(99)00192-8.

Mercone, D., Thomson, J., Croudace, I.W., Siani, G., Paterne, M., and Troelstra, S., 2000, Duration of S1, the most recent sapropel in the eastern Mediterranean Sea, as indicated by accelerator mass spectrometry radiocarbon and geochemical evidence: Paleoceanography, v. 15, p. 336–347, .

Rohling, E.J., Cane, T.R., Cooke, S., Sprovieri, M., Bouloubassi, I., Emeis, K.-C., Schiebel, R., Kroon, D., Jorissen, F.J., Lorre, A., and Kemp, A.E.S., 2002a, African monsoon variability during the previous interglacial maximum: Earth and Planetary Science Letters, v. 202, p. 61–75, doi: 10.1016/S0012–821X(02)00775–6.

Rohling, E.J., Mayewski, P.A., Hayes, A., Abu-Zied, R.H., and Casford, J.S.L., 2002b, Holocene atmosphere-ocean interactions: records from Greenland and the Aegean Sea: Climate Dynamics, v. 18, p. 587–593, doi; 10.1007/s00382-001-0194-8.

Figure DR1. Left I) Down-core records of different geochemical proxies through S5 for core LC21. Shaded area represents the visual extent of the dark-coloured sapropel S5 sediments. It corresponds to a partly laminated, benthic azoic interval indicating persistent sea-floor anoxia. A: δ^{18}O records for the summer mixed layer dwelling *Globigerinoides ruber* (white) (grey dashed line) and top intermediate water dwelling *Neogloboquadrina pachyderma* (dextral) (black dashed line) planktonic foraminifera. B: δ^{13}C records for *G. ruber* (white) and *N. pachyderma*. The isotopic records (δ^{18}O and δ^{13}C) of *G. ruber* (grey solid line) and *N. pachyderma* (black solid line) were lowess smoothed (tension 0.04 and 0.05, respectively) in order to highlight main trends. C: SST reconstructions based on the long-chain alkenone unsaturation index (black solid line). D: Organic carbon content (Corg, wt%) (black filled area). E: Isorenieratene abundance calculated with respect to the total amount of sediment (grey filled area). Right II) Linear (grey line) and polynomial (black line) fits through the primary correlation markers (grey open diamonds), using ODP 971A as the independent variable ("bench mark") and LC21 as dependent variable. Black open circles represent secondary correlation markers. Big + and grey blocks indicate the visual extent of the dark-coloured sapropel sediments. The time scale on the right is based on the correlation between major shifts in the $\delta^{18}O_{ruber}$ at sapropel onset and termination and the onset and termination of the humid period in Soreq Cave (Rohling et al., 2002a).

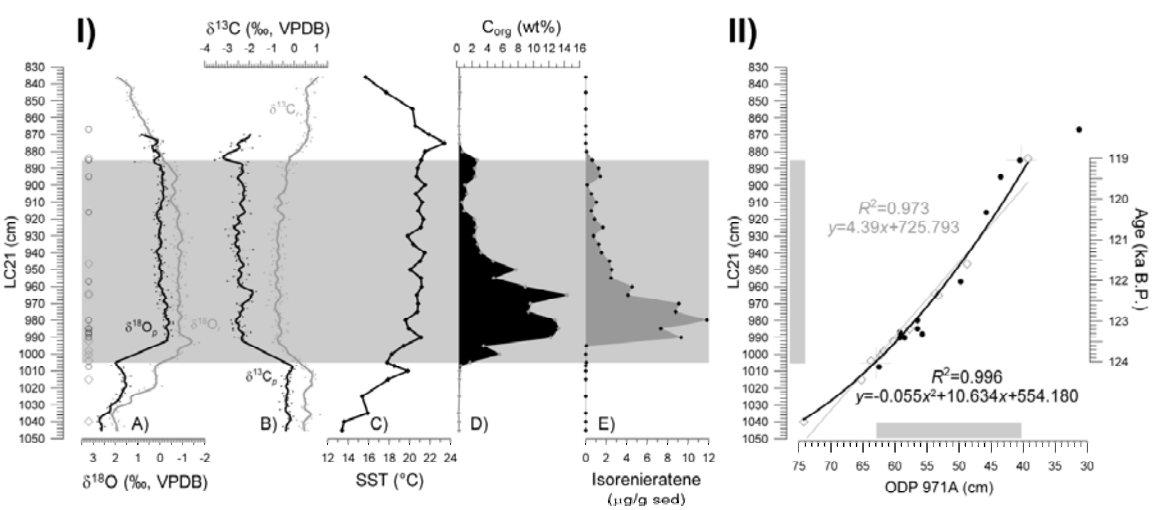

<u>Figure DR2</u>. A: alkenone-based SST (open circles), $\delta^{18}O_{pachyderma}$ (black line), and $\delta^{18}O_{ruber}$ (grey line) records in 971A; B: alkenone-based SST (open circles), $\delta^{18}O_{pachyderma}$ (black line), and $\delta^{18}O_{ruber}$ (grey line) records in LC21; C: $\delta^{13}C_{pachyderma}$ (black line), and $\delta^{13}C_{ruber}$ (grey line) records in 971A; D: $\delta^{13}C_{pachyderma}$ (black line), and $\delta^{13}C_{ruber}$ (grey line) records in LC21. Labels identify correlation markers (Table DR1).

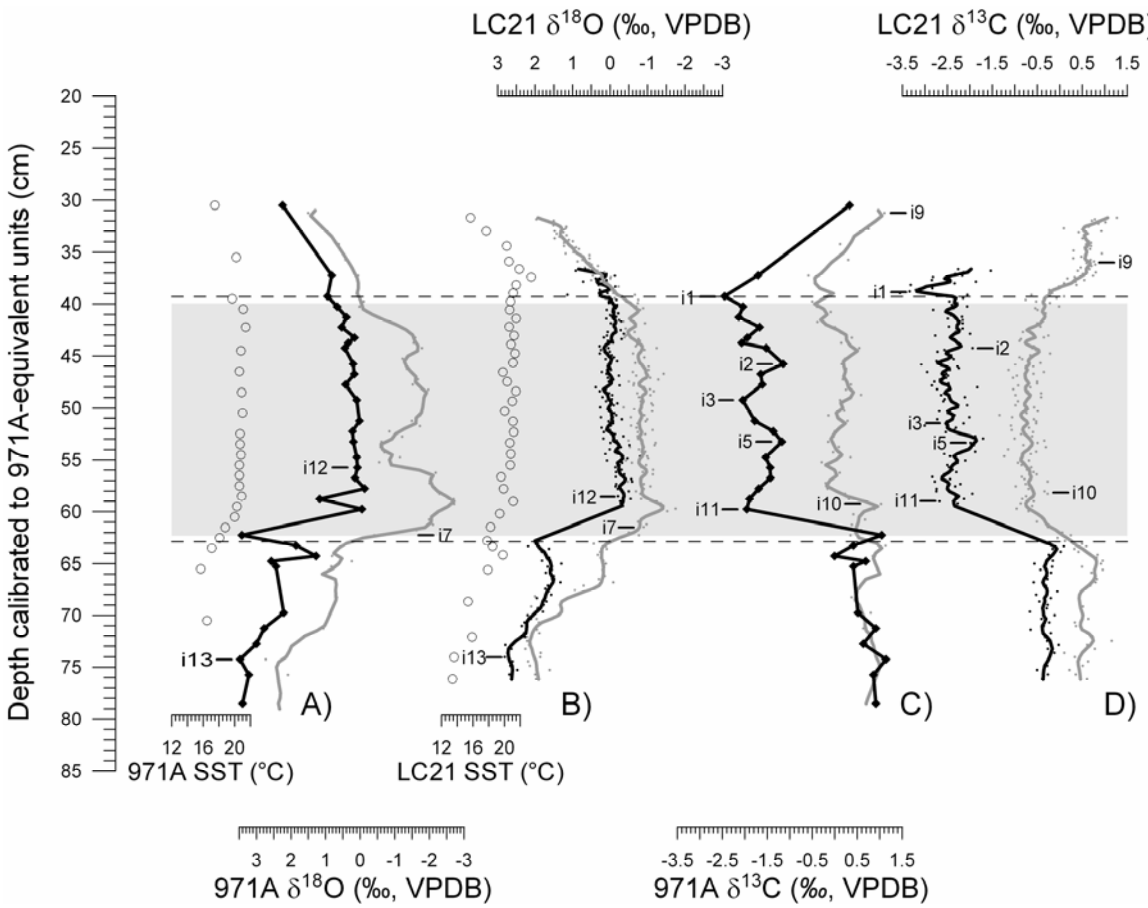

<u>Table DR1</u>. List of the primary and secondary correlation markers.

Correlation point	Species/stable isotope/org. geochem.	Definition	Confidence	971A Depth	LC-21 Depth
i1	*N. pachyderma* $\delta^{13}C$	prominent isotopic depletion peak at sapropel cessation	primary	39.25	884.00
f2	*G. sacculifer* faunal	sample before species reappears	primary	48.75	946.50
f4	*G. scitula* faunal	species no longer present (zero abundance)	primary	53.25	965.00
i5	*N. pachyderma* $\delta^{13}C$	first prominent isotopic enrichment peak	primary	53.75	964.00
f5	*G. sacculifer* faunal	species no longer present (zero abundance)	primary	57.75	985.00
f6	*N. pachyderma* faunal	sample before species reappears after short absence	primary	60.25	992.00
f8	*G. inflata* faunal	species no longer present (zero abundance)	primary	61.75	998.00
i7	*G. ruber* $\delta^{18}O$	mid-point of isotopic depletion at sapropel onset	primary	62.25	1000.5
f9	pink *G. ruber* faunal	sample before the species appears	primary	63.75	1004.0
f10	*N. pachyderma* faunal	prominent peak below sapropel preceding sharp drop in abundance	primary	62.25	1015.0
i13	*N. pachyderma* $\delta^{18}O$	shoulder before depletion trend	primary	74.25	1040.0
i9	*G. ruber* $\delta^{13}C$	prominent peak in isotopic enrichment after sapropel	secondary	31.25	867.00
i2	*N. pachyderma* $\delta^{13}C$	second prominent isotopic enrichment peak	secondary	45.75	916.00
i3	*N. pachyderma* $\delta^{13}C$	prominent isotopic depletion between i1 and i11	secondary	49.75	957.00
i12	*N. pachyderma* $\delta^{18}O$	first major depletion	secondary	55.75	988.00
i10	*G. ruber* $\delta^{13}C$	shoulder during isotopic depletion in basal third of the sapropel	secondary	59.25	987.00
i11	*N. pachyderma* $\delta^{13}C$	prominent isotopic depletion peak after sapropel onset	secondary	59.25	990.00
isor1	isorenieratene org. geochem.	last peak in isorenieratene abundance	secondary	43.50	895.00
isor2	isorenieratene org. geochem.	Highest value in isorenieratene abundance after the sapropel onset	secondary	56.50	980.0
isor3	isorenieratene org. geochem.	sample before preceding isorenieratene occurrence	secondary	58.50	990.0
C_{org} 1	C_{org} org. geochem.	last sample at the sapropel termination where C_{org}<2%	secondary	40.50	885.00
C_{org}2	C_{org} org. geochem.	peak in C_{org} after sapropel onset	secondary	62.50	1007.0
C_{org}3	C_{org} org. geochem.	last sample before C_{org}>1% at the sapropel onset	secondary	56.50	985.00
top black				40.25	885.00
base black				63.00	1005.0